Supplementary Information (SI) for Inorganic Chemistry Frontiers.

Halogen-bond induced polar multilayer hybrid perovskites for efficient self-driven X-ray detection

Haotian Wen,[a,b] Minmin Wang,[a,b] Xin Dong,[b] Zhijin Xu,[b] Yaru Geng,[b] Jie Qin,[a,b] Junhua Luo,[b,d] Min Zhang,[a,c,d]* and Lina Li[a,b,d]*

[a] College of Chemistry, Fujian University, Fuzhou 350116, China.

[b] State Key Laboratory of Functional Crystals and Devices, Fujian Institute of Research on the Structure of Matter, Chinese Academy of Sciences Fuzhou, Fujian, 350002, China.

[c] State Key Laboratory of Structural Chemistry, Fujian Science & Technology Innovation Laboratory for Optoelectronic Information of China, Fujian Institute of Research on the Structure of Matter, Chinese Academy of Sciences, Fuzhou 350002, China.

[d] Fujian Science & Technology Innovation Laboratory for Optoelectronic Information of China Fuzhou, Fujian, 350108, China.

*Corresponding Author: Lina Li. Email Address: lilina@fjirsm.ac.cn

Min Zhang. Email Address: zhangmin@fjirsm.ac.cn

Experimental Procedures

Materials: $Pb(Ac)_2$ (99%, Aladdin), methylamine (MA, 29%, Aladdin), hydroiodic acid (HI, 48%, Aladdin), Aminobutanol (99%, Aladdin). All the chemicals were bought and used without further purification.

Synthesis. $Pb(Ac)_2$ (2.27 g, 6 mmol) was dissolved in 48% aqueous HI solution (10 mL) by heating to boiling under constant magnetic stirring to give a yellowish solution. Subsequent addition of Aminobutanol (0.36 g, 4 mmol) and MA(0.45 g, 4 mmol) to the hot solution formed yellowish precipitation. Dissolved under heating and stirring, and kept the solution boiling under reflux for 5 minutes to fully react and obtained a dark yellow solution. Finally, black-red crystals were obtained after the solution was cooled to room temperature at a rate of 1 K/day.

Powder X-ray diffraction. Powder X-ray diffractions (PXRD) were performed on a Rigaku MiniFlex 600 diffractometer at room temperature. The diffraction patterns were collected in the 2θ range of 5°−40° with a step size of 0.5 °/min. The experimental PXRD patterns match fairly well with the simulated data based on the single-crystal structure, which confirm the pure phase of **1**.

Optical property measurements. The UV absorptions in solid state were measured at room temperature on a PE Lambda 900 UV-Visible spectrophotometer.

Theoretical Calculation. The electrostatic potentials (ESP) for the ligands were calculated by the Gaussian 09 package at the B3LYP/6-31G level with the DFT-D3 method. Density functional theory (DFT) calculations were carried out with the CASTEP program in the Materials Studio software. The exchange and correlation effects are treated by the Perdew-Burke-Ernzerh method of generalized gradient approximation. The core-electrons interaction between the ion cores and the electrons is described in terms of the norm-conserving pseudopotential.

X-Ray Detection. The current-voltage (*I-V*) traces and current-time (*I-t*) curves of **1** single-crystal device were recorded by a Keithley 6517B high-precision electrometer. An Amptek Mini-X2 X-ray tube with the silver target (maximum power 4 W) was used as the X-ray source. The maximum X-ray photons energy is 50 keV and the peak intensity is at 22 keV. The dose rate of the X-ray tube was modulated by changing its tube current and measured by a Radical Accu-Gold X-ray dosimeter attached to the 10×6-180 ion chamber in an integrating mode.

Detection performance measurements: We tested the detection performance of the above device under polarized light incident parallel to the c-axis direction at zero bias. The responsivity (R) and the corresponding detectivity (D*) of the device (Figure 2d) were measured at zero bias, calculated from the following equations：

$$R = \frac{I_{\text{light}} - I_{\text{dark}}}{P \times S}$$

$$D^* = \frac{R \times \sqrt{S}}{\sqrt{2\text{e}I_{\text{dark}}}}$$

where I_{light} is the photocurrent, I_{dark} is the dark current, P is the incident light power, S is the effective area and e is the electron charge.

Calculation of $\mu\tau$ Product: The $\mu\tau$ product was derived by fitting the photoconductivity of a single crystal detector of **1** under X-ray illumination using the modified Hecht equation,

$$I = \frac{I_0 \mu\tau V}{L^2}\left[1 - \exp\left(\frac{-L^2}{\mu\tau V}\right)\right]$$

where I is the photocurrent, I_0 is the saturated photocurrent, L is the distance between electrodes, V is the applied bias, μ is carrier mobility, and τ is carrier lifetime.

Calculations of Sensitivity (S): S is defined as the collected charge per unit area under X-ray irradiation and can be determined by

$$S = \frac{J_{\mathrm{ph}} - J_{\mathrm{d}}}{D}$$

where J_{ph} and J_{d} represent the current densities under X-ray irradiation and in the dark, respectively, and D denotes the dose rate.

Calculation of signal-to-noise ratio: The signal-to-noise ratio (SNR) was calculated as

$$SNR = \frac{\bar{I}_{\mathrm{ph}} - \bar{I}_{\mathrm{d}}}{\sqrt{\frac{1}{N}\sum_{\mathrm{i}}^{\mathrm{n}}\left(I_{\mathrm{i}} - \bar{I}_{\mathrm{ph}}\right)^2}}$$

Where the I_{i} denotes measured photocurrent, and $\bar{I}_{ph}, \bar{I}_{d}$ is the average of measured photocurrent and dark current, respectively. Following the definition given by the IUPAC, the dose rate that generates an SNR of 3 is regarded as the detection limit of an X-ray detector.

Calculation of Dark Current Drift (I_{drift}): The dark current drift is determined by the following equation

$$I\mathrm{drift} = \frac{J_{\mathrm{t}} - J_0}{E\mathrm{t}}$$

Where J_{t} and J_0 are the recorded beginning and final dark current densities, respectively, E is the electric field strength, and t is the total dark current test time.

Figures and tables

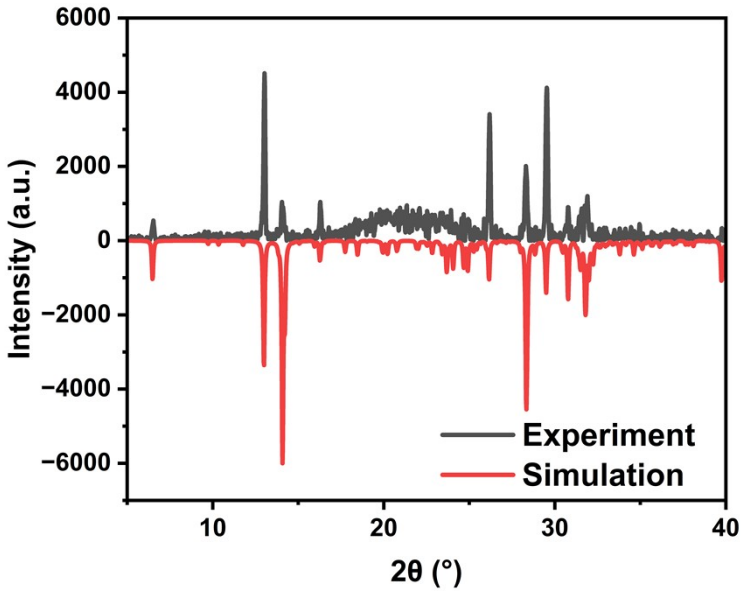

Figure S1. Experimental and simulated PXRD patterns for **1** at room temperature.

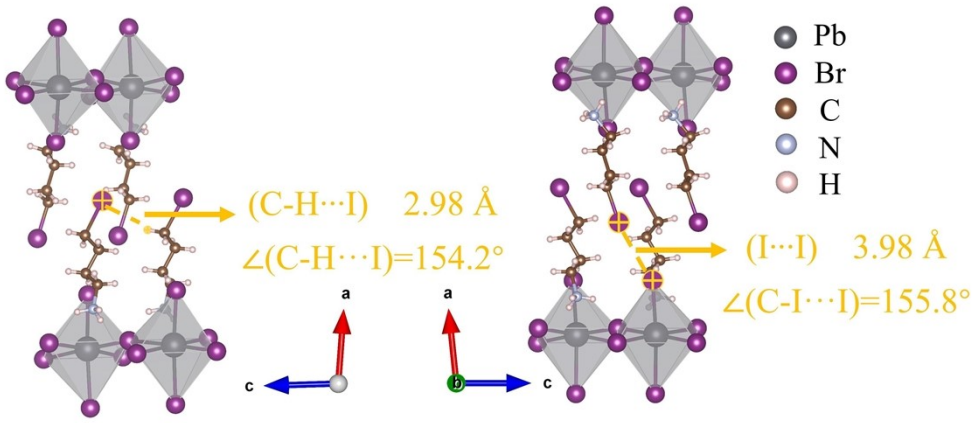

Figure S2. Geometrical parameters for iodine-involved halogen bonds in the crystal.

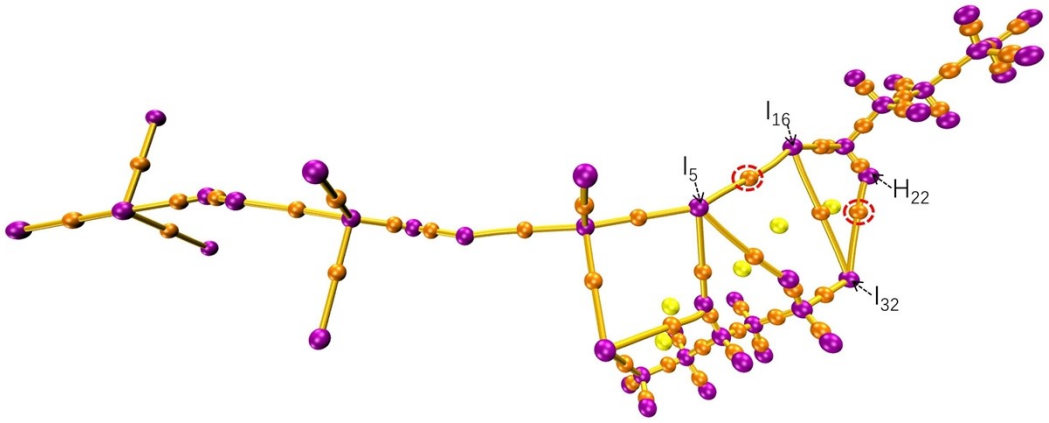

	ρ_{BCP}	$\nabla^2\rho(r)$	H(r)	G(r)	V(r)
$H_{22}\cdots I_{32}$	0.0067	0.017	0.0006	0.0036	-0.0029
$I_5\cdots I_{16}$	0.126	-0.053	-0.068	0.055	-0.123

Figure S3. The QTAIM analysis of **1** (The purple spheres represent (3,-3) critical points, which essentially coincide with the positions of the atomic nuclei. The orange spheres correspond to bond critical points, while the yellow spheres denote ring critical points. The brown lines indicate the bond paths).

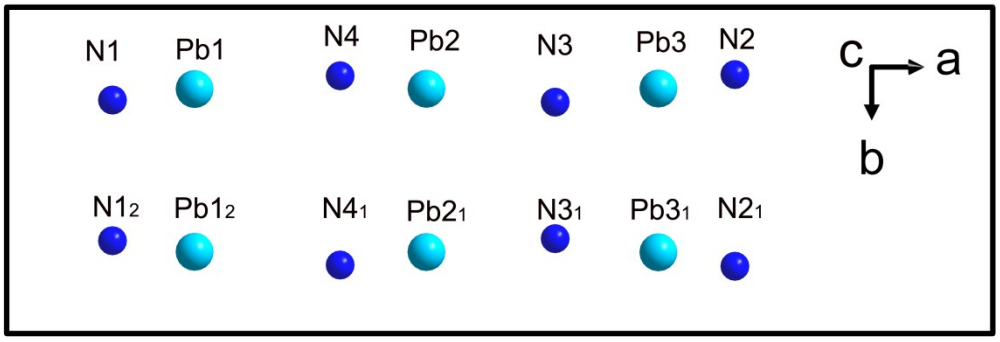

Figure S4. Point-charge model for calculating the polarization of **1** at 290 K. Hydrogen atoms are omitted for clarity.

Table 1. Atom coordinate for cell of **1** (290K).

Atoms	Atoms coordinate		Coordinate of charge center
Pb	Pb1(0.19055,0.25067,0.95588) Pb2(0.42572,0.24994, 0.03430) Pb3(0.66095,0.24915, 0.11329)	$Pb1_2$(0.19055,0.74933,0.45588) $Pb2_1$(0.42572,0.75006,0.53430) $Pb3_1$(0.66095,0.75085,0.61329)	(0.42574, 0.5, 0.45115)
N	N1 (0.1073, 0.28448, 0.3671) N2 (0.73853, 0.2063, 0.6413) N3 (0.55627, 0.29089, 0.538) N4(0.33825,0.21002, 0.5366)	$N1_2$ (0.1073, 0.71552, 0.8671) $N2_1$ (0.73853, 0.7937, 0.1413) N b_2 (0.55627, 0.70911, 0.038) N b_4(0.33825, 0.77899, 0.0366)	(0.43509, 0.5, 0.39575)

$P_{s\ a\text{-axis}} = [(-e \times 0.42574) \times 6 \times 4/3 + (e \times 0.43509) \times 8] \times a / V$

$= [0.0748 \times 1.6 \times 10^{-19} \times 27.3848 \times 10^{-10}\ C\ m]/V$

$= 3.28 \times 10^{-29}\ C\ m / (2162.65 \times 10^{-30}\ m^3)$

$= 1.51 \times 10^{-2}\ C\ m^{-2}$

$|P_s| = 1.51 \times 10^{-2}\ C\ m^{-2} = 1.51\ \mu C\ cm^2$

$P_{s\ c\text{-axis}} = [(-e \times 0.45115) \times 8 + (e \times 0.39557) \times 8] \times c / V$

$= [0.5558 \times 1.6 \times 10^{-19} \times 8.8216 \times 10^{-10}\ C\ m]/V$

$= 7.84 \times 10^{-29}\ C\ m / (2162.65 \times 10^{-30}\ m^3)$

$= 3.62 \times 10^{-2}\ C\ m^{-2}$

$|P_s| = 3.62 \times 10^{-2}\ C\ m^{-2} = 3.62\ \mu C\ cm^2$

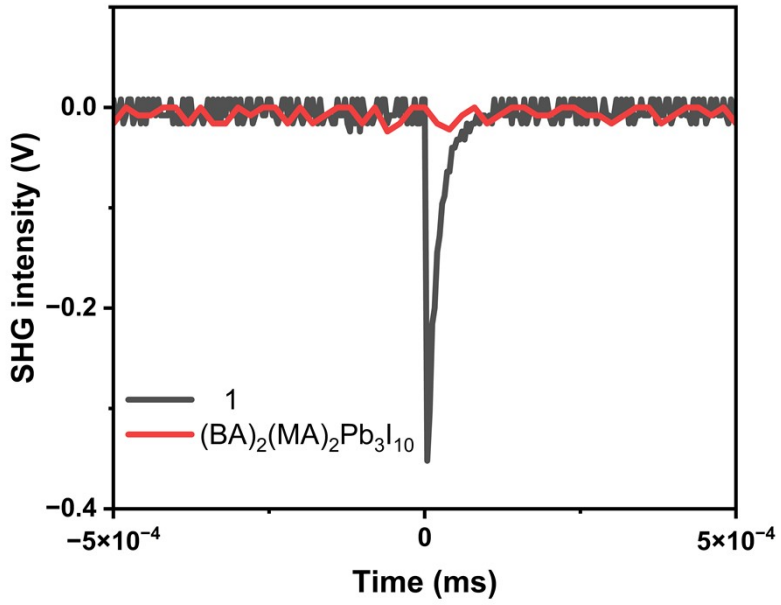

Figure S5. The SHG signals for the **1** and $(BA)_2(MA)_2Pb_3I_{10}$ at room temperature.

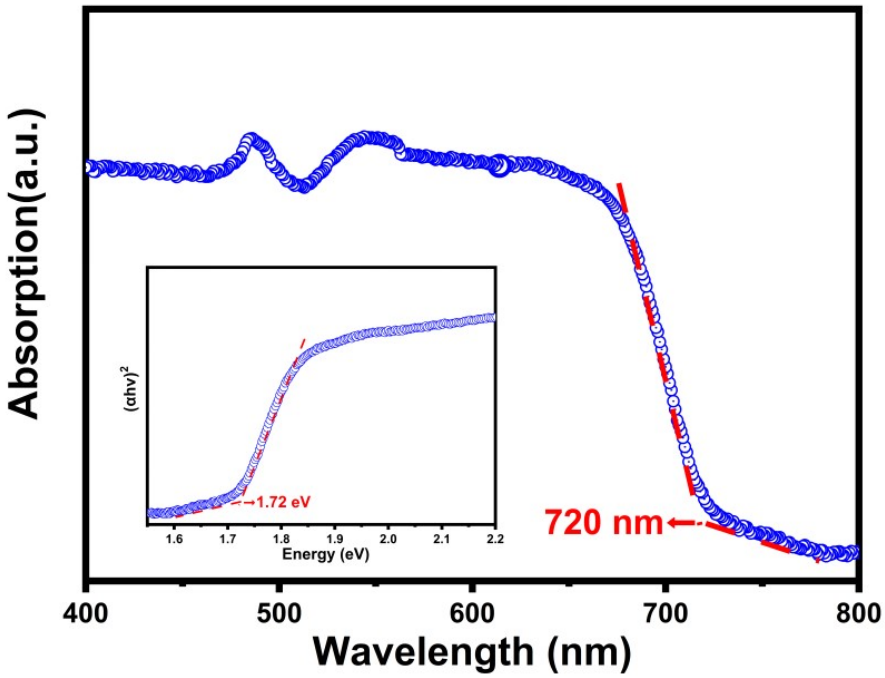

Figure S6. Absorption spectra of 1. Inset: calculation of the bandgap by Tauc plot.

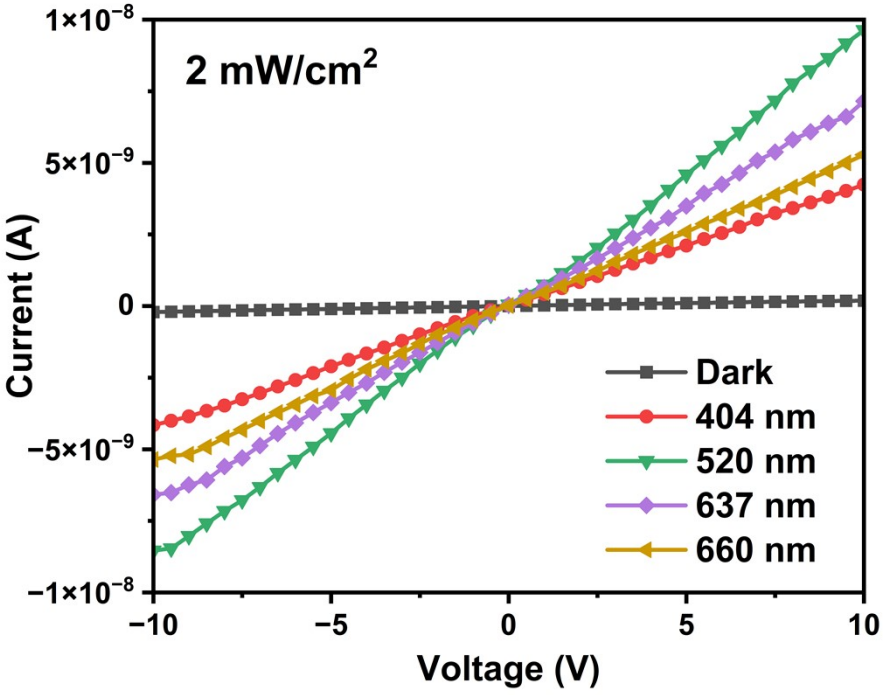

Figure S7. Photoresponse of **1** at wavelengths from 404 to 660 nm under 2 mW/cm^2 illumination.

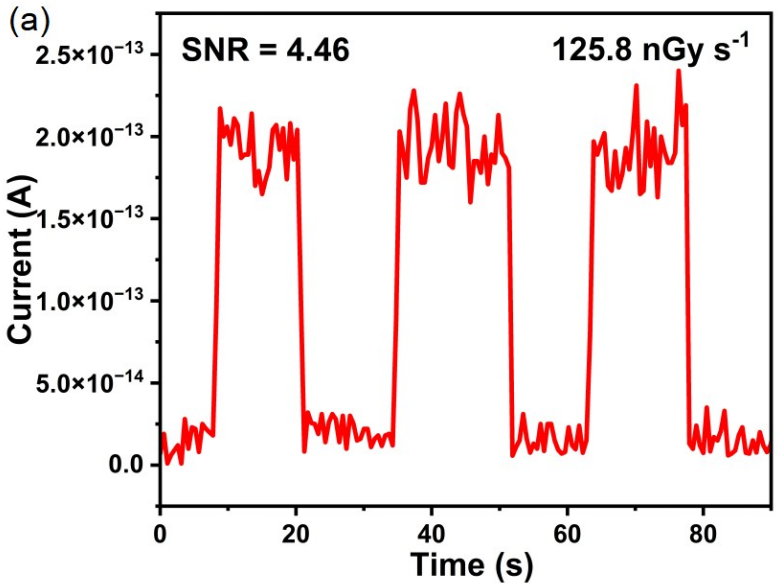

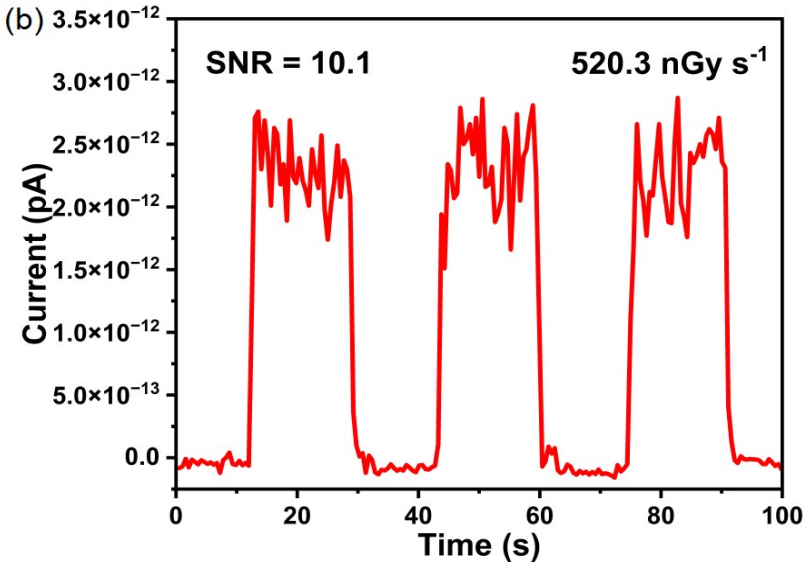

Figure S8. Photocurrent response of **1** detector to X-ray under lower dose rates a) and higher dose rates b) at 0 V bias